Evaluation of the GOES-R ABI LAP Retrieval Algorithm Using the *GOES-13* Sounder

YONG-KEUN LEE, ZHENGLONG LI, AND JUN LI

Cooperative Institute for Meteorological Satellite Studies, University of Wisconsin–Madison, Madison, Wisconsin

TIMOTHY J. SCHMIT

NOAA/NESDIS/Center for Satellite Applications and Research, Camp Springs, Maryland

(Manuscript received 4 February 2013, in final form 15 September 2013)

ABSTRACT

A physical retrieval algorithm has been developed for deriving the legacy atmospheric profile (LAP) product from infrared radiances of the Advanced Baseline Imager (ABI) on board the next-generation Geostationary Operational Environmental Satellite (GOES-R) series. In this study, the GOES-R ABI LAP retrieval algorithm is applied to the *GOES-13* sounder radiance measurements (termed the *GOES-13* LAP retrieval algorithm in this study) for its validation as well as for potential transition of the *GOES-13* LAP retrieval algorithm for the operational processing of GOES sounder data. The *GOES-13* LAP retrievals are compared with five different truth measurements: radiosonde observation (raob) and microwave radiometer–measured total precipitable water (TPW) at the Atmospheric Radiation Measurement Cloud and Radiation Testbed site, conventional raob, TPW measurements from the global positioning system–integrated precipitable water NOAA network, and TPW measurements from the Advanced Microwave Scanning Radiometer for Earth Observing System (AMSR-E). The results show that with the GOES-R ABI LAP retrieval algorithm, the *GOES-13* sounder provides better water vapor profiles than the National Centers for Environmental Prediction (NCEP) Global Forecast System (GFS) forecast fields at the levels between 300 and 700 hPa. The root-mean-square error (RMSE) and standard deviation (STD) of the *GOES-13* sounder TPW are consistently reduced from those of the GFS forecast no matter which measurements are used as the truth. These substantial improvements indicate that the GOES-R ABI LAP retrieval algorithm is well prepared to provide continuity of quality to some of the current GOES sounder products, and the algorithm can be transferred to process the current GOES sounder measurements for operational product generation.

1. Introduction

The Geostationary Operational Environmental Satellite (GOES) sounders have been observing the continental United States (CONUS) and adjacent ocean area since 1994 at 18 infrared (IR) channels approximately between 3.7 and 14.7 μm, providing quality hourly radiances and derived products (Menzel and Purdom 1994; Menzel et al. 1998; Daniels et al. 2001; Hillger et al. 2003, 2010). The operationally derived products from the GOES sounders include clear-sky radiances, temperature/moisture profiles, total precipitable water (TPW), stability indices, cloud-top pressure, and water vapor tracked winds (Velden et al. 1997; Schmit et al. 2002; Jin et al. 2008; Li et al. 2008, 2009). The GOES sounder products have been shown useful for nowcasting and forecasting of weather events (Menzel et al. 1998; Schrab 1998; Li et al. 2008, 2009) and monitoring temperature and moisture changes in the preconvective atmospheric environment (Schmit et al. 2002).

The first of the next-generation GOES series (the GOES-R) is scheduled for launch in 2015 and the Advanced Baseline Imager (ABI) will be the primary instrument on GOES-R for observing Earth's weather and climate (Schmit et al. 2005). As an imager, the capability of ABI will be significantly improved over that of the current GOES imagers considering that the GOES-R ABI will have finer spatial resolution (2 km for infrared channels) and a faster scan rate (15 min for full disk, plus 5 min for CONUS, and 30 s for mesoscale regions) compared to the current GOES imagers. However, the GOES-R satellite will not carry the

Corresponding author address: Yong-Keun Lee, CIMSS, University of Wisconsin, 1225 West Dayton St., Madison, WI 53706.
E-mail: yklee@ssec.wisc.edu

DOI: 10.1175/JTECH-D-13-00028.1

Hyperspectral Environmental Suite (HES) dedicated to acquire high spatial and temporal resolution temperature and moisture profiles that are the key to weather forecasting (Schmit et al. 2005). Instead, Schmit et al. (2008) showed that ABI, along with a numerical model initial profile, has a similar capability to provide legacy atmospheric temperature and moisture profiles, which could be adequate substitutes for current GOES sounder legacy products. Jin et al. (2008) developed the GOES-R ABI legacy atmospheric profiles (LAP) retrieval algorithm. They tested the algorithm using the European Organisation for the Exploitation of Meteorological Satellites (EUMETSAT)'s Spinning Enhanced Visible and Infrared Imager (SEVIRI) measurements as proxy and concluded that the GOES-R ABI LAP will provide useful legacy products with a quality similar to that of the current GOES sounder product. Xie et al. (2013) evaluated the GOES-R ABI LAP products with the SEVIRI data as a proxy by comparing with in situ measurements obtained over the open ocean from multiple years of the National Oceanic and Atmospheric Administration (NOAA) Aerosols and Ocean Science Expeditions (AEROSE). They found that the GOES-R ABI LAP retrievals agree reasonably well with the AEROSE radiosonde observations and provide improved profiles of temperature and water vapor compared to the National Centers for Environmental Prediction (NCEP) Global Forecast System (GFS) forecast output.

Unlike the earlier validation efforts that used SEVIRI proxy data (e.g., Jin et al. 2008; Xie et al. 2013), we use *GOES-13* sounder data to validate the algorithm over the relevant coverage area. This change is needed to validate the algorithm performance for mesoscale weather forecasting over CONUS, which is one of the primary applications of the ABI. The sounding retrieval over the Atlantic Ocean region by Xie et al. (2013) is relatively easy because of its homogeneous ocean surface. The CONUS region is generally a more challenging environment because of the complexity of the land surface.

Since the ABI-like atmospheric moisture retrievals (Jin et al. 2008; Schmit et al. 2008; Xie et al. 2013) have proven to be more useful than the temperature retrievals, this study will focus on validation of the moisture and moisture-related products, including moisture profiles, TPW, and the lifted index.

A brief description of the *GOES-13* LAP retrieval algorithm and an introduction of the truth data are given in section 2. Section 3 describes the validation results of the *GOES-13* LAP products compared with the truth data. The summary and discussion are given in section 4.

2. The *GOES-13* LAP retrieval algorithm and the truth data

a. *The* GOES-13 *LAP retrieval algorithm*

In this study, the *GOES-13* LAP retrieval algorithm is defined as the GOES-R ABI LAP retrieval algorithm applied to the *GOES-13* sounder measurements, and the retrieval products are called the *GOES-13* LAP products.

The physical retrieval algorithm for *GOES-13* LAP uses regression-derived temperature/water vapor profiles as the first guess (Jin et al. 2008, 2009). A synthetic regression technique is used to generate the regression coefficients. The radiosonde observation (raob) atmospheric profiles (6280 profiles) are employed from the SeeBor database (Seemann et al. 2003, 2008) within the current GOES satellite coverage: latitudes between 80.4663°N and 80.4663°S and longitudes between 155.8618°W and 5.8618°E. This dataset includes surface skin temperature and surface IR emissivities (Seemann et al. 2003, 2008). The *GOES-13* sounder brightness temperatures (BTs) are simulated with the Community Radiative Transfer Model (CRTM version 2.0.2) developed by NOAA's Joint Center for Satellite Data Assimilation (Weng et al. 2005; Chen et al. 2010, 2012). The radiosonde temperature/water vapor profiles are predictands, and the simulated *GOES-13* sounder 15-channel BTs combined with forecast temperature/water vapor profiles, surface pressure, land/ocean flag, latitude, and month are used as predictors to generate the regression coefficients. The forecast profiles are generated using the raob profiles with the addition of suitable noise. Local zenith angle (between 0° and 80°) classification is used to reduce the impacts from the viewing angle.

The regression coefficients are applied to the 15 *GOES-13* sounder channels (Table 1) and the GFS forecast fields (temperature/water vapor profiles) to provide the first guess, similar to Li et al. (2008). This regression-based sounding retrieval serves as the first guess for the physical iterations. The 15 *GOES-13* sounder channels, from channels 1 (14.7 μm) to 15 (4.45 μm), are used in both the regression process and the physical iterative algorithm (Table 1). It should be noted that the *GOES-13* sounder has several more CO_2 sensitive channels than the ABI.

The NCEP GFS 3-, 6-, and 9-h forecast fields are available every 6 h (0000, 0600, 1200, and 1800 UTC) over the entire globe at a horizontal resolution of 0.5° and 26 vertical levels. They are spatially interpolated to *GOES-13* sounder grids and to 101 vertical levels and temporally interpolated to every nominal hour of *GOES-13* sounder measurements. When there are multiple GFS forecasts available for a specific nominal hour, the most recent one will be taken.

TABLE 1. *GOES-13* sounder bands used for the *GOES-13* LAP algorithm.

Band number	Wavelength (μm)	Purpose	Corresponding ABI band number
1	14.70	Temperature sounding	
2	14.40	Temperature sounding	
3	14.10	Temperature sounding	
4	13.90	Temperature sounding	
5	13.40	Temperature sounding	16
6	12.70	Temperature sounding	
7	12.00	Surface temperature	15
8	11.00	Surface temperature	14
9	9.70	Total ozone	12
10	7.40	Water vapor	10
11	7.00	Water vapor	9
12	6.50	Water vapor	8
13	4.57	Temperature sounding	
14	4.52	Temperature sounding	
15	4.45	Temperature sounding	

The *GOES-13* LAP physical iterative algorithm derives temperature and water vapor profiles from satellite observed radiances using a one-dimensional variational (1DVAR) iterative technique (Rodgers 1976; Ma et al. 1999; Li et al. 2008). During iterations, the atmospheric profile in the form of a vector $\mathbf{X}$ is adjusted from the first guess $\mathbf{X}^b$ to minimize a cost function $J(\mathbf{X})$ (Rodgers 1976). The cost function is defined as follows:

$$J(\mathbf{X}) = [\mathbf{Y}^m - F(\mathbf{X})]^{\mathrm{T}}\mathbf{E}^{-1}[\mathbf{Y}^m - F(\mathbf{X})] + [\mathbf{X} - \mathbf{X}^b]^{\mathrm{T}}\gamma\mathbf{B}^{-1}[\mathbf{X} - \mathbf{X}^b], \quad (1)$$

where $\mathbf{B}$ is the error covariance matrix of the first guess $\mathbf{X}^b$, $\mathbf{E}$ is the error covariance matrix of the observation vector, $\mathbf{Y}^m$ is the measurement, $F(\mathbf{X})$ is the forward radiative transfer operator, and γ is the regularization parameter (or smoothing factor) used for solution convergence and stability (Li et al. 2000). Superscripts T and -1 are the matrix transpose and matrix inverse, respectively. The background error covariance matrix $\mathbf{B}$ is calculated based on the differences between the radiosonde dataset and the spatially and temporally collocated GFS forecast products. The matrix $\mathbf{E}$ includes the errors of the observed BTs (BT error in the instrument) and the uncertainty of the radiative transfer model. Because of the difficulty in quantifying the correlative errors, only the diagonal element is retained. The cost function poses two conditions on the retrieval: 1) the retrieval is constrained to the first guess, and 2) the calculated BT based on the retrieval is constrained to the observed BT.

With Eq. (1) and the Newtonian method,

$$\mathbf{X}_{n+1} = \mathbf{X}_n - [\nabla^2 J(\mathbf{X}_n)]^{-1}\nabla^2 J(\mathbf{X}_n), \quad (2)$$

the following iterative form is derived:

$$\delta\mathbf{X}_{n+1} = (F_n'^T \cdot \mathbf{E}^{-1} \cdot F_n' + \gamma\mathbf{B}^{-1})^{-1} \cdot F_n'^T \cdot \mathbf{E}^{-1} \cdot (\delta\mathbf{Y}_n + F_n' \cdot \delta\mathbf{X}_n), \quad (3)$$

where $\delta\mathbf{X}_n = \mathbf{X}_n - \mathbf{X}^b$, $\delta\mathbf{Y}_n = \mathbf{Y}^m - F(\mathbf{X}_n)$, n is the iteration step, and F' is the tangent linear operative (Jacobian) of forward model F. During the physical retrieval iteration, the first guess is modified in a controlled manner to fit the calculated BTs to the *GOES-13* observed BTs. More details of the procedure in the GOES-R ABI LAP retrieval algorithm employed in this study can be found in Li et al. (2010) and Jin et al. (2008).

The main difference in the retrieval algorithms between this study and Li et al. (2008) is the radiative transfer model. This study employs the CRTM while Li et al. (2008) used the Pressure-Layer Fast Algorithm for Atmospheric Transmittance (PFAAST). As shown in the cost function given in Eq. (1), a radiative transfer model plays a critical role during the physical retrieval iterations. Jin et al. (2011) showed that the CRTM is better with temperature/moisture retrievals than PFAAST, and the CRTM is superior in brightness temperature simulations especially at 7.3 μm (a moisture channel) than PFAAST. Thus, the use of the CRTM to improve our retrievals in this study may result in some differences relative to the Li et al. (2008) study, as shown below in section 3c.

b. The truth data

1) THE MEASUREMENTS FROM THE ARM CART SITE

The Atmospheric Radiation Measurement (ARM) Cloud and Radiation Testbed (CART) at the Southern Great Plains (SGP) site is the largest and most extensive climate research facility in the world located at 36.61°N, 97.47°W (Stokes and Schwartz 1994). The ARM CART is the first field measurement site established by U.S. Department of Energy (DOE)'s ARM program. The SGP site was selected as the first ARM field measurement site because of its high variability of weather conditions, large seasonal variability of temperature, moisture and precipitation, spatially homogeneous terrain, and easy accessibility. Since 1992, instrumentation and data processing capabilities have been incrementally added at the ARM CART site. Recently, the ARM CART site has been selected as a site in the Global Climate Observing System (GCOS) Reference Upper-Air Network (GRUAN) to provide long-term, highly accurate measurements of the atmospheric profiles. The 6-hourly raob and 30-s TPW estimates inferred from the microwave radiometer (MWR) at the ARM

TABLE 2. Measurement characteristics for TPW truth data obtained for the period between 11 Feb 2011 and 30 Aug 2012. AMSR-E data availability is limited to the period between 11 Feb 2011 and 4 Oct 2011 due to operations issues.

	Observation frequency	Spatial resolution or coverage	*GOES-13* collocation criteria
MWR	30 s	36.61°N, 97.47°W	±30 min 0.2° in radius
GPS sites	30 min	251 sites over eastern CONUS	±30 min 0.2° in radius
ARM CART site (raob)	6 h	36.61°N, 97.47°W	±30 min 0.2° in radius
Conventional raob sites	12 h*	59 sites over eastern CONUS	±30 min 0.2° in radius
AMSR-E	2–3 times per day	24 km over eastern CONUS ocean	±30 min 10 km in radius

* Nominal conventional raob launches occur routinely at 0000 and 1200 UTC with occasional launches at 0600 and 1800 UTC.

CART site are used as ground truth in this study because they are considered stable and accurate (Liljegren 1995; Immler et al. 2010). These data are obtained from the ARM Data Archive for the period from 11 February 2011 to 30 August 2012 (Table 2) to match the *GOES-13* sounder data. Note that the *GOES-13* sounder radiance observations have been available since 11 February 2011. Raob temperature/water vapor profiles have been widely used to evaluate remotely sensed profiles (Fuelberg and Olson 1991; Rao and Fuelberg 1998; Jin et al. 2008). MWR TPW has been used as the truth data (Schmit et al. 2002, 2008; Li et al. 2008; Hanesiak et al. 2010). The temporal and spatial collocation of the *GOES-13* LAP products and the GFS forecast products with the ARM CART site measurements and other truth measurements is described in section 2c. The number of samples selected is the number of the *GOES-13* sounder fields of view (FOVs) temporally and spatially collocated with the truth data. The sample sizes are 6338 and 1079 for MWR TPW and raob, respectively (Table 3). The location of the ARM CART site is shown in Fig. 1.

2) CONVENTIONAL RAOB

Of all the conventional raob sites, 59 sites overlap with the *GOES-13* sounder over the eastern CONUS (Fig. 1). The conventional raob temperature/water vapor profiles and TPW integrated from the conventional raob water vapor profile are used for the *GOES-13* LAP product validation for the period between 11 February 2011 and 30 August 2012. The sample size is 25 529 (Table 3).

3) THE GPS TPW MEASUREMENTS

The NOAA ground-based global positioning system–integrated precipitable water (GPS–IPW) network (Birkenheuer and Gutman 2005) TPW measurement is employed as another independent source of TPW measurement. The GPS TPW measurement is available every 30 min and it is collected for the period from 11 February 2011 to 30 August 2012 from 251 NOAA ground-based GPS–IPW network sites over the eastern CONUS (blue circles in Fig. 1). The sample size is 1 010 609 (Table 3).

4) THE AMSR-E TPW MEASUREMENTS

The ARM CART site measurements, the conventional raobs, and the GPS TPW measurements provide reliable resources for validating the *GOES-13* LAP product over land. Such data are not usually available over the ocean. However, microwave radiometer data taken from polar orbiting satellites provide a reliable resource over the ocean (Fetzer et al. 2006; Jin et al. 2008). The Advanced Microwave Scanning Radiometer for the Earth Observing System (AMSR-E) instrument provided TPW measurements over the ocean at a 24-km horizontal resolution. The selected measurement coverage of AMSR-E is shown in Fig. 1. The sample size is 3 847 196 (Table 3). Since AMSR-E ended its operation at 0726 UTC 4 October 2011, the AMSR-E TPW data are collected for the period between 11 February 2011 and 4 October 2011.

TABLE 3. Statistical comparison between TPW derived from the *GOES-13* LAP algorithm and GFS forecast using five truth datasets for the period between 11 Feb 2011 and 30 Aug 2012. The AMSR-E comparison period ended on 4 Oct 2011.

	GOES-13 LAP				GFS forecast					
	BIAS (mm)	STD (mm)	RMSE (mm)	Corr coef	BIAS (mm)	STD (mm)	RMSE (mm)	Corr coef	Truth mean (mm)	No. of selected samples
MWR	0.84	2.03	2.19	0.9869	0.88	2.42	2.57	0.9803	19.98	6338
ARM raob	1.52	2.50	2.93	0.9820	1.56	2.73	3.15	0.9762	20.01	1079
Conventional raob	0.28	3.10	3.12	0.9713	0.29	3.28	3.29	0.9680	19.59	25 529
GPS	0.38	2.25	2.29	0.9847	0.20	2.44	2.45	0.9814	19.52	1 010 609
AMSR-E	−0.83	2.21	2.36	0.9819	−1.52	2.45	2.89	0.9773	30.27	3 847 196

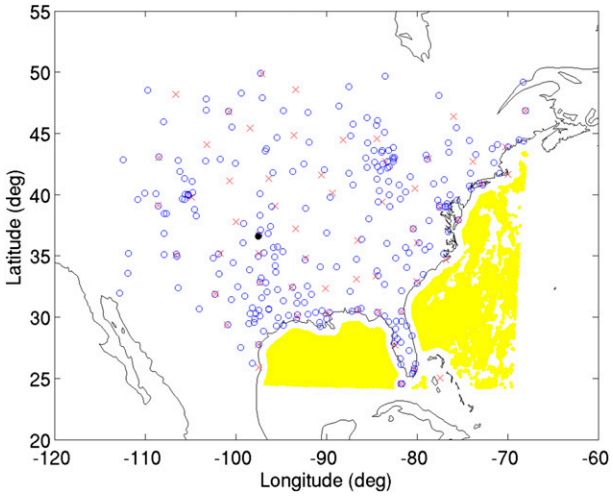

FIG. 1. The ARM CART site (black dot), 59 conventional raob locations (red cross), 251 GPS–IPW NOAA network locations (blue circle), and AMSR-E locations (yellow area) are indicated over the eastern CONUS.

c. *Collocation*

To compare the *GOES-13* LAP products and the GFS forecast products with the truth measurements, the closest *GOES-13* sounder FOV to the location of each truth measurement is searched within a 0.2° radius (except AMSR-E) and within a 30-min measurement time difference (Table 2). The closest *GOES-13* sounder FOV to an AMSR-E FOV is searched within a 10-km radius. MWR-measured TPWs found within ±30 min are averaged and used as the truth in this study. Only clear-sky *GOES-13* sounder FOVs are considered and the clear sky is determined by the *GOES-13* sounder cloud mask based on Schreiner et al. (2001).

3. Validation results

a. *Temperature/water vapor profile*

There are two truth datasets included in this study for temperature/water vapor profile comparison: the raobs at the ARM CART site and the conventional raob sites. ARM raobs have an overall better quality than conventional raobs (Turner et al. 2003) and more frequent measurements (4 times a day at the ARM CART site and usually 2 times a day at the conventional raob sites). The conventional raob sites offer a greater geographical distribution.

Figure 2 shows the standard deviation (STD) and mean bias (BIAS) of the *GOES-13* LAP and the GFS forecast profiles compared with ARM raobs (Figs. 2a,b) and conventional raobs (Figs. 2c,d). Both the temperature STD and BIAS reveal very small differences (mostly less than 0.1 K) between the retrieval and the GFS forecast against either ARM raobs or conventional raobs (Figs. 2a,c). The GFS forecast temperature shows excellent quality regarding both STD and BIAS. The BIAS value of the GFS forecast temperature is less than 1 K in magnitude (between 300 and 700 hPa) at both the ARM CART site and the conventional raob sites. These results demonstrate that the *GOES-13* LAP retrieval algorithm has difficulty improving the temperature profiles over the GFS forecast despite six CO_2 absorption channels in the troposphere. This is true for all traditional low spectral resolution IR sounders [including the GOES sounder and the High Resolution Infrared Radiation Sounder (HIRS) or imagers with limited sounding capability (including SEVIRI and ABI)]. The main reason for this is the significant progress in assimilating satellite CO_2 channel radiances in the past decades. As a result, the NWP forecast depicts the temperature field quite well, leaving little room for those instruments to provide additional temperature information.

Figures 2b and 2d show the STD and BIAS of the relative humidity profile at the ARM CART site and the conventional raob sites, respectively. Unlike the temperature profile in Figs. 2a and 2c, the retrieval significantly reduces both the relative humidity STD and BIAS from the GFS forecast for the vertical levels between 300 and 700 hPa. The *GOES-13* LAP relative humidity STD is well below 15% between 300 hPa and the surface compared with the ARM raob and with the conventional raob. The *GOES-13* LAP relative humidity BIAS is well below 18% when compared with both the ARM raob and the conventional raob as the truth. Such moisture information comes from the three *GOES-13* sounder water vapor channels (7.4, 7.0, and 6.5 μm; Table 1). The ABI has three similar water vapor channels (7.34, 6.95, and 6.19 μm), but with a much smaller spatial resolution (nadir: 2 km of ABI versus 10 km of *GOES-13* sounder). Therefore, it is expected that when the GOES-R ABI LAP is averaged to nominal 10-km spatial resolution, it will provide similar or even better improvement in moisture information over the GFS forecast. Since the GOES-R ABI LAP relative humidity profile requirement (Li et al. 2010) is 18% in both accuracy and precision for the levels below 300 hPa, the results shown in Figs. 2b and 2d indicate that the GOES-R ABI LAP humidity profile will meet the requirement. In Jin et al. (2008), the SEVIRI data are used as a proxy of the ABI data. Even though SEVIRI has only two water vapor channels (6.2 and 7.35 μm), the moisture information has been significantly improved from the background input [European Centre for Medium-Range Weather Forecasts (ECMWF) forecast fields].

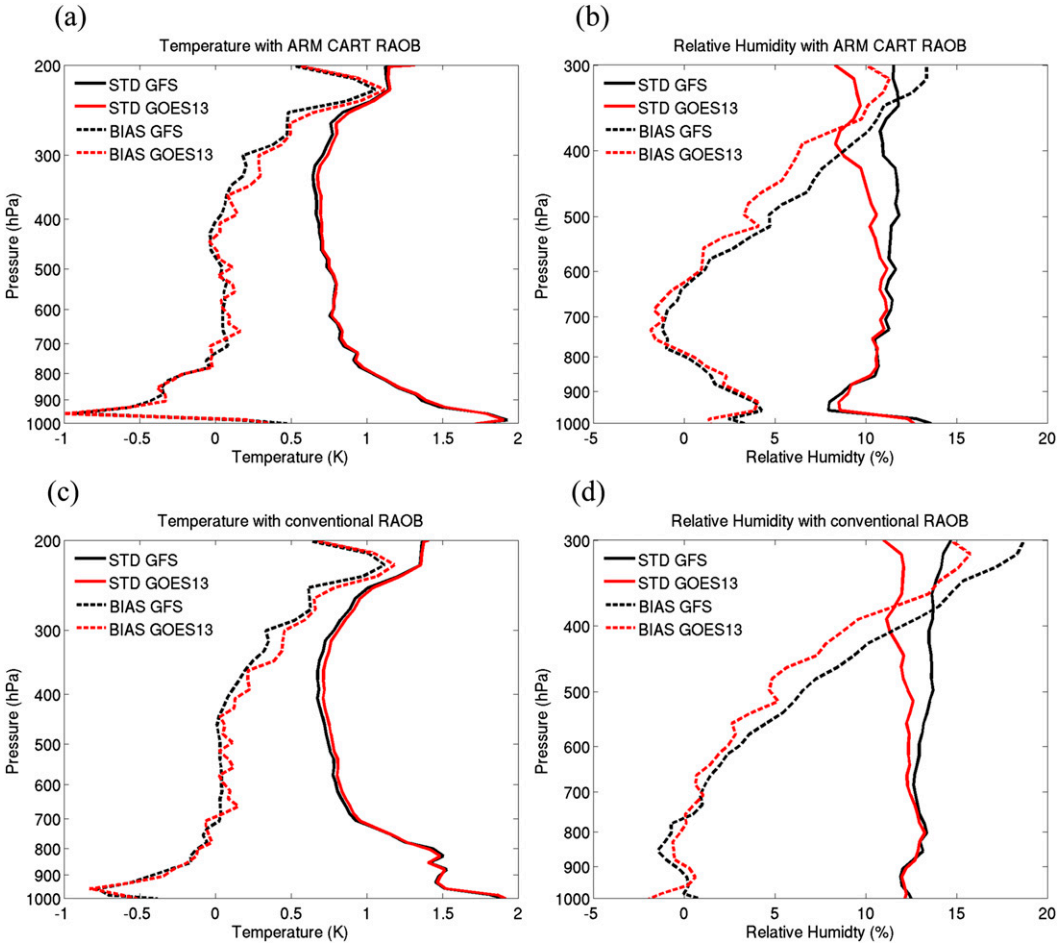

FIG. 2. The STD and BIAS profiles of the *GOES-13* LAP (a) temperature and (b) relative humidity, and the GFS forecast (c) temperature and (d) relative humidity compared to the ARM CART (top) raob (sample size is 1079) and the (bottom) conventional raob (sample size is 25 529). Comparison is valid during the period between 11 Feb 2011 and 30 Aug 2012.

Reale et al. (2012) showed the statistics of the NCEP GFS 6-h forecast water vapor compared with in situ measurements based on the NOAA Products Validation System (NPROVS). The NCEP GFS 6-h forecast temperature and water vapor were compared with radiosonde measurements. In their study, the BIAS of the water vapor fraction profile is within ±20% of the absolute value below 400 hPa, and the BIAS of the temperature profile is within ±1 K in absolute value. Compared to their results, the BIAS values of the NCEP GFS forecast temperature and water vapor are within a reasonable range in this study. All these results indicate that the GFS forecast depicts the moisture field less well than the temperature field. Part of the reason for that is the current assimilation technique does not allow optimal utilization of moisture information from satellite radiances; most of the moisture and surface channels (sensitive to moisture in the lower atmosphere) are either abandoned or weight reduced in the assimilation (Collard et al. 2010).

The sounding retrieval is able to extract additional moisture information compared with the NWP forecast. As shown in Schmit et al. (2008), an IR hyperspectral geostationary sounder may provide more accurate atmospheric vertical temperature/moisture information than the current GOES sounder or ABI instrument, which will allow forecasters and numerical prediction models to use a more detailed three-dimensional atmospheric structure.

b. Total precipitable water

TPW is a useful product for weather forecasters. TPW is the amount of liquid water (in millimeters) in a column of the atmosphere if all the water vapor in that column were condensed. High values of TPW in clear skies are often associated with the preconvective

environment prior to severe storms, which are capable of producing hail, tornadoes, heavy precipitation, and flash floods. It is one of the critical variables used by forecasters in the weather forecasting discussions at the National Weather Service's Weather Prediction Center when there are expectations of flash flooding or severe weather. Many satellite-derived TPW products are available in real time worldwide. For example, the National Environment Satellite, Data, and Information Service (NESDIS) provides a real-time blended TPW product as one of the precipitation products, and the Cooperative Institute for Meteorological Satellite Studies (CIMSS) Convective Development Nearcasting Model (CCDNM) provides precipitable water products. The EUMETSAT Network of Satellite Application Facilities (NWC SAF; support to nowcasting and very short-range forecasting) also provides precipitable water products in real time.

Chen et al. (2008) showed that the assimilation of Moderate Resolution Imaging Spectroradiometer (MODIS) TPW data into the Weather Research and Forecasting (WRF) model slightly improved simulated rainfall over the region of interest in southern Oklahoma for a severe thunderstorm case in June 2004, and the hurricane track or intensity was improved by the use of MODIS TPW data for Hurricane Isadore over the ocean in September 2002. Liu et al. (2011) revealed the positive impacts of MODIS- and the Atmospheric Infrared Sounder (AIRS)-retrieved TPW on WRF simulations of Hurricane Emily (July 2005). They showed that the assimilation of MODIS TPW into the WRF model improved the hurricane track, intensity, and 10-m wind field.

There are five independent TPW measurements used as truth in this study: the MWR-measured TPW at the ARM CART site (MWR TPW), the raob TPW integrated from the raob water vapor profile at the ARM CART site (ARM raob TPW), the raob TPW integrated from the conventional raob water vapor profiles (conventional raob TPW), the GPS-measured TPW (GPS TPW) over the CONUS land area, and the AMSR-E-measured TPW (AMSR-E TPW) over the eastern CONUS ocean. See Fig. 1 for the locations of these measurements. TPWs integrated from the *GOES-13* LAP and the GFS forecast water vapor profiles are compared to these five truth datasets.

Table 3 shows the statistics (including RMSE, STD, BIAS, and correlation coefficient) of the TPWs from the *GOES-13* LAP retrieval and the GFS forecast compared to the five truths for the period 11 February 2011 through 30 August 2012 (AMSR-E data are collected for the period 11 February 2011 through 4 October 2011). The RMSE and STD values of the *GOES-13* LAP TPW are below 2.4 mm, except for raob TPWs at the ARM CART site and the conventional raob sites, and most of the BIAS values are below 0.86 mm in magnitude, except when using ARM raob TPW as the truth. The GOES-R ABI LAP TPW requirements are 1 mm in accuracy and 3 mm in precision (Li et al. 2010). Again, considering that the ABI instrument has three water vapor channels similar to those on the *GOES-13* sounder but with much finer spatial and temporal resolutions, the statistical values in Table 3 suggest the GOES-R ABI LAP TPW will meet the requirements.

The agreement levels are different between the retrieval and the truth measurements in Table 3 due to several possible reasons: 1) the truth TPW measurements have different qualities (i.e., accuracy and precision) (Pacione et al. 2002; Mattioli et al. 2005); 2) measurement time lengths are different—the raob is taken over a period of time while others are all instant (snapshot) measurements; and 3) measurement spatial resolutions are different—MWR and raob are point measurements, while the retrieval, GPS, and AMSR-E are over a relatively large area.

After the physical retrieval, all RMSE and STD results are reduced and correlation coefficients are increased from the GFS forecast, no matter which measurement is used as the truth. The minimum reduction of RMSE is 0.16 mm (2.45–2.29 mm) with the GPS TPW as the truth, and the maximum reduction is 0.53 mm (2.89–2.36 mm) with the AMSR-E TPW as the truth. The minimum reduction of STD is 0.19 mm (2.44–2.25 mm) with the GPS TPW as the truth, and the maximum reduction is 0.39 mm (2.42–2.03 mm) with the MWR TPW as the truth. These results indicate the GOES-R ABI LAP algorithm is effective to improve the GFS forecast TPW using the *GOES-13* sounder measurements.

TPWs from several independent instruments, such as MWR, GPS, raob, and AMSR-E, have been compared in previous studies (Pacione et al. 2002; Mattioli et al. 2005; Kazumori et al. 2012). These comparisons show that TPWs from the independent measurements agree to within 1 mm in accuracy and some instruments are drier (or wetter) than others. Mattioli et al. (2005) compared TPWs from MWR, GPS, and raob at the ARM CART site and showed that the instruments agreed to within 1 mm in TPW STD and the TPW becomes drier (in order from least to most dry: MWR, raob, and GPS). Since a GPS permanent station is operating at the ARM CART site, the *GOES-13* LAP TPW statistics compared against TPWs of MWR, raob, and GPS at the ARM CART site should provide results similar to Mattioli et al. (2005). The *GOES-13* LAP TPW BIAS against GPS TPW at the ARM CART site is 1.88 mm (for the same time periods, not shown), indicating that

the GPS TPW is drier than the MWR TPW (*GOES-13* LAP TPW BIAS of 0.84 mm). The ARM raob TPW is in the middle (*GOES-13* LAP TPW BIAS of 1.52 mm). These results agree with Mattioli et al. (2005). Kazumori et al. (2012) revealed that the AMSR-E TPW is wetter than the TPWs measured by radiosonde and GPS, which is consistent with the negative bias of the *GOES-13* LAP TPW against the AMSR-E TPW in Table 3.

While the GFS forecast TPW is found to be of good quality relative to the truth datasets (i.e., low RMSE, STD, and BIAS errors and high correlation coefficients), the *GOES-13* LAP TPW retrievals are found to be superior in most aspects, indicating that the *GOES-13* sounder does indeed provide additional moisture information that can improve weather forecasts using current nowcasting and assimilation techniques (e.g., Chen et al. 2008; Liu et al. 2011).

1) MONTHLY VARIATION

A reliable algorithm should perform consistently in different months. Figure 3 shows monthly RMSE, STD, BIAS, and the sample size of the *GOES-13* LAP TPW and the GFS forecast TPW compared to the five truths. The STD values are large during the summer months (June, July, and August) and small during the winter months (December, January, and February). These results are consistent with those found by Pacione et al. (2002) when comparing independent TPW measurements (MWR, GPS, and raob).

Figure 3 depicts that the RMSE and STD found for the *GOES-13* LAP retrievals relative to all five truth datasets are consistently lower than those found for the GFS forecast in most months. This suggests that additional moisture information is being extracted from the *GOES-13* sounder relative to that found in the GFS forecasts.

Unlike RMSE and STD, which are consistently improved by the *GOES-13* LAP algorithm, the TPW BIAS shows mixed results. The monthly variation in the TPW BIAS depends on which truth measurement is selected. If MWR TPW is used as truth, the *GOES-13* LAP algorithm improves the BIAS in 10 out of 12 months. When the BIAS is increased, the RMSE could be increased. There are three occasions in Fig. 3 when the RMSE is increased after the retrieval: July with the ARM raob TPW as the truth, as well as February and October with the AMSR-E TPW as the truth. The increased TPW BIAS is the reason for these three exceptions (note that the STD in the *GOES-13* LAP TPW is all reduced from the GFS forecast TPW).

Dai et al. (2002) showed that the GPS-measured TPW has a diurnal variation with peak mean TPW values appearing during the daytime in the summer over CONUS.

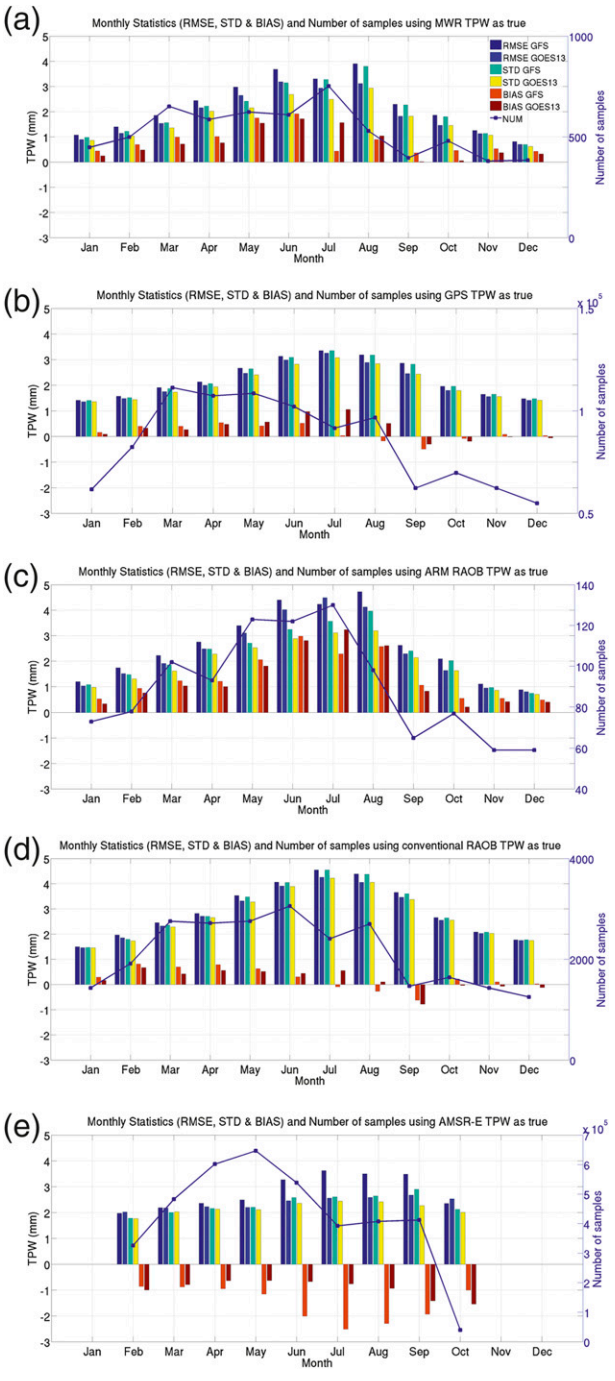

FIG. 3. Monthly variation of TPW RMSE, STD, BIAS, and number of samples for the *GOES-13* LAP retrieval and the GFS forecast. The truth data are (a) the ARM CART site MWR-measured TPW, (b) GPS-measured TPW, (c) the ARM CART site raob TPW, (d) 59 conventional raob TPW, and (e) AMSR-E-measured TPW. During the period between 11 Feb 2011 and 30 Aug 2012, (a)–(d) are valid, and (e) is valid during the period between 11 Feb 2011 and 4 Oct 2011.

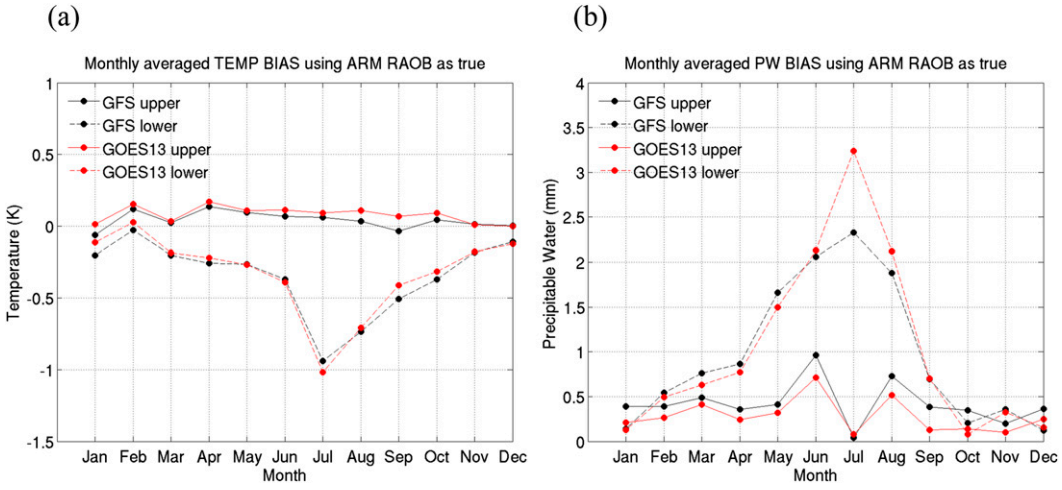

FIG. 4. Monthly variation in the BIAS of (a) mean temperature (vertically averaged) and (b) PW for the upper troposphere between 300 and 800 hPa and the lower troposphere below 800 hPa using raob at the ARM CART site as the truth for the period between 11 Feb 2011 and 30 Aug 2012.

The retrieval in this study may not be able to capture the diurnal variation in TPW during the summer months [shown in section 3b(2)]. Dai et al. (1999, 2002) and Wang et al. (2002) suggested likely reasons for the diurnal variation of TPW: 1) surface evapotranspiration, 2) mesoscale low-level horizontal convergence of moisture, 3) large-scale advection, 4) large-scale atmospheric vertical motion, and 5) localized moist convection. Considering that the *GOES-13* LAP TPW has a larger BIAS than the NCEP GFS forecast during the daytime in the summer months over land (Fig. 6), further investigations of these factors are needed to discover why the retrieval quality during that time is affected.

As given in section 2a, two conditions are placed on the retrieval by the cost function (Jin et al. 2008; Li et al. 2010): 1) the retrieval is constrained to the first guess, and 2) the calculated BT based on the retrieval is constrained to the observed BT. These conditions suggest the importance of the quality of the background inputs (the GFS forecast temperature/water vapor profiles) and of the quality *GOES-13* sounder BT measurements. Remember that the first guess is obtained using the background (the GFS forecast temperature/water vapor profiles) and the *GOES-13* sounder BT measurement as predictors through regression. Therefore, the quality of the retrieved TPW may be affected by two possible factors: 1) the quality of the GFS forecast temperature/water vapor profiles, and 2) the quality of the *GOES-13* sounder BT measurement.

Figure 4 shows the monthly BIAS of the GFS forecast temperature profile (vertically averaged) and precipitable water (PW) in the lower troposphere at the ARM CART site. PW is calculated in the same way as TPW except that the integration is for the lower troposphere (between the surface and 800 hPa) and the upper troposphere (between 800 and 300 hPa) in Fig. 4. The averaged BIAS of the *GOES-13* LAP temperature profile shows variations similar to the averaged BIAS of the GFS forecast temperature profile for both the upper troposphere and the lower troposphere.

The BIAS of the *GOES-13* LAP PW in the upper troposphere is generally reduced from that of the GFS forecast in the upper troposphere, which is clear from Fig. 2b. In July, the BIAS values of both the GFS forecast temperature (−0.94 K, vertically averaged) and PW (2.29 mm) below 800 hPa are worse compared with those in other months in Fig. 4, and the *GOES-13* LAP TPW BIAS is 0.95 mm larger than the GFS forecast TPW BIAS causing the retrieved TPW RMSE to be degraded from the GFS forecast TPW RMSE (Fig. 3c). However, the BIAS value of the retrieval in July in Fig. 3c appears to be normal against the ARM raob TPW. The *GOES-13* LAP TPW BIAS shows a consistent and smooth monthly trend (large in summer and small in winter) in Fig. 3c, despite the smaller GFS forecast TPW BIAS in July. This monthly trend of the *GOES-13* LAP TPW BIAS is also shown against the MWR TPW and GPS TPW.

In Fig. 4, it appears that the quality of the GFS forecast temperature/water vapor profiles is more variable in the lower troposphere than in the upper troposphere. Since the *GOES-13* LAP algorithm has limited capability to improve the GFS temperature profile and the *GOES-13* sounder provides little useful moisture information at levels below about 700 hPa, large errors in the GFS forecast temperature and water vapor profiles cannot be adequately corrected with the LAP algorithm

and the retrieved moisture is likely to have a large bias. To determine the impact of the BIAS of the temperature/water vapor in the first guess on the retrieval, two separate experiments have been conducted by changing either temperature or water vapor amount (not shown): 1) 0.5-K increase in the GFS forecast temperature below 800 hPa, and 2) 5% decrease in the GFS forecast water vapor below 800 hPa. While the 0.5-K increase in the GFS forecast temperature in the lower troposphere results in the retrieved TPW BIAS increase (0.25 mm in July) from the *GOES-13* LAP retrieval, the 5% decrease (or about 1.15 mm decrease of PW in July) in the GFS forecast water vapor in the lower troposphere induces the retrieved TPW BIAS decrease (0.9 mm in July) from the *GOES-13* LAP retrieval. Although these experiments reveal that the quality of the background (the GFS forecast fields) affects the physical retrieval quality, similar consistent monthly trends of the *GOES-13* LAP TPW BIAS are still observed in the experiments. Since the background inputs (the GFS forecast temperature/water vapor profiles) and the *GOES-13* sounder BT measurements are the two main sources of data for the retrieval, the *GOES-13* sounder BT calibration needs to be further investigated to discover how it is related to the quality of the *GOES-13* LAP retrieval.

2) Diurnal variation

Geostationary satellites have the advantage of staying over a permanent location on Earth, which makes it possible to observe the same area continuously. This advantage allows investigations in diurnal variation over the observed area.

Figure 5 shows the hourly diurnal variations of RMSE, STD, and BIAS; the sample size for TPW calculated from the *GOES-13* LAP; and the GFS forecast compared to the five truths. Since the ARM raob, conventional raob, and the AMSR-E observations are not available hourly (see Table 2), the statistics are only shown at the hours when they are available. The occasional conventional raob at 0600 and 1800 UTC (147 and 150 samples, respectively) are also included in Fig. 5d.

Most of the time during a 24-h cycle, the *GOES-13* LAP retrieval algorithm is effective in reducing TPW RMSE from the GFS forecast in Fig. 5. However, it appears that the *GOES-13* LAP algorithm has more difficulty during the daytime than during the nighttime. During the daytime, there are some exceptions where the retrieved TPW has a larger RMSE than the GFS forecast TPW, such as 1500–1600 UTC in Fig. 5a, 1600–2000 UTC in Fig. 5b, and 1800 UTC in Figs. 5c and 5d. (The local time over CONUS is 4–8 h behind UTC.) When the AMSR-E TPW is used as the truth in Fig. 5e, the *GOES-13* LAP algorithm always shows a smaller RMSE than the GFS forecast TPW over all available times. However, the reduction from 1700–2000 UTC is clearly less pronounced than other times. These results indicate that the *GOES-13* LAP retrieval algorithm is

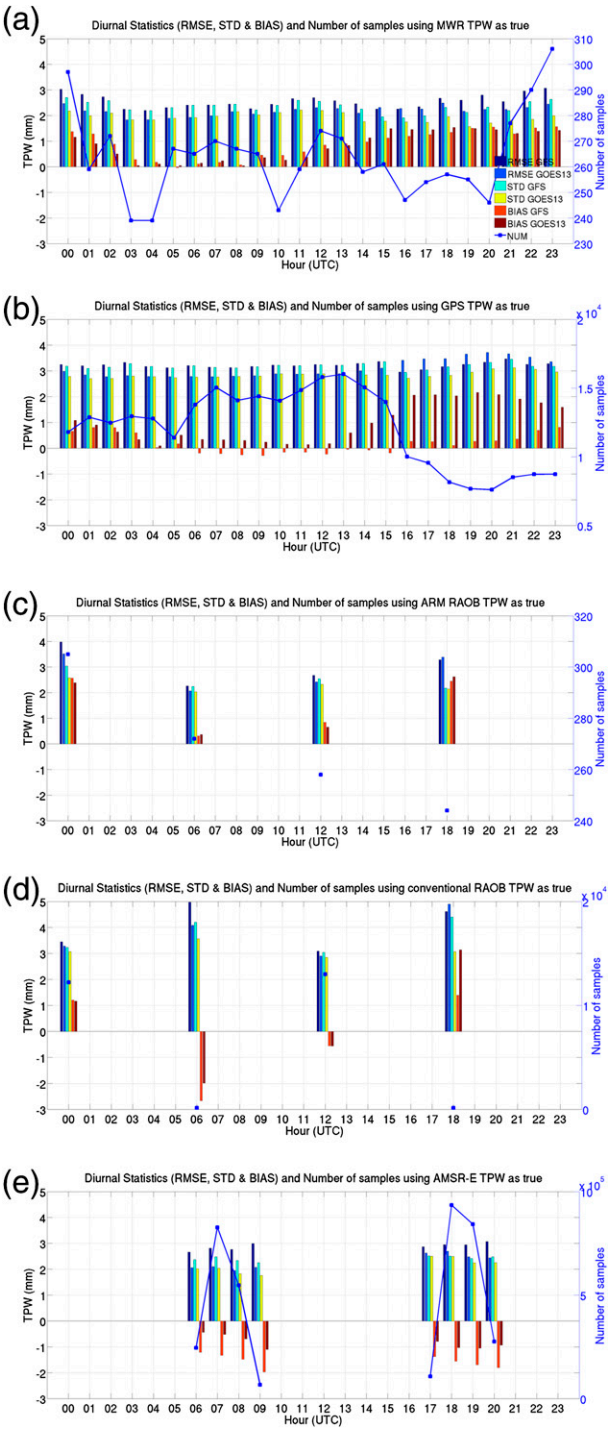

FIG. 5. As in Fig. 3, but for diurnal variation.

less efficient at improving the GFS forecast in the daytime. The degraded performance is mainly because of the algorithm's difficulty in improving the TPW BIAS. In Fig. 5, the *GOES-13* LAP TPW BIAS shows a clear diurnal variation over land. The TPW STD, on the other hand, does not show any strong diurnal pattern; the retrieval always shows a smaller TPW STD than the GFS forecast, regardless of which observation or what time is used as the truth. It is postulated that an improved instrument spectral resolution would improve the retrieval quality (Schmit et al. 2009; Sieglaff et al. 2009). One reason is that high spectral resolution observations will better allow for determining the surface emissivity.

The *GOES-13* LAP TPW BIAS increase during the daytime happens mostly in the summer months (May, June, July, and August), when compared to the truth datasets over the CONUS land. Figure 6 shows the monthly BIAS of the *GOES-13* LAP and the GFS forecast TPW at 1600 UTC using the MWR TPW and GPS TPW as the truths and at 1800 UTC using the raob TPWs at the ARM CART site and the conventional raob sites and the AMSR-E TPW as the truths.

Figure 7 shows the diurnal BIAS variation in the GFS forecast, the *GOES-13* LAP temperature profile (vertically averaged), PW for the upper troposphere (between 300 and 800 hPa), the lower troposphere (below 800 hPa) at the ARM CART site, and the conventional raob sites. Similar to the monthly variation in Fig. 4, the BIAS of the *GOES-13* LAP and the GFS forecast fields show similar variations for both the upper and lower tropospheres. At 1800 UTC (daytime), the BIAS of both the GFS forecast temperature (0.76 K at the conventional raob sites) and PW (1.70 mm at the ARM CART site) below 800 hPa are relatively large compared to other times in Fig. 7. The *GOES-13* LAP PW BIAS in the lower troposphere is increased from the GFS forecast both at the ARM CART site and the conventional raob sites at this time, and thus the *GOES-13* LAP TPW BIAS is increased from the GFS forecast at both the ARM CART site and the conventional raob sites in Figs. 5c and 5d.

Two separate experiments have been conducted to examine the impacts of the background inputs (GFS forecast fields) by changing either the temperature or water vapor amount in the lower atmosphere (not shown): 1) a 0.5-K decrease in the GFS forecast temperature below 800 hPa at the conventional raob sites, and 2) a 5% decrease in the GFS forecast water vapor below 800 hPa at the ARM CART site. The second experiment is the same as that of the monthly variation in Fig. 4. The 0.5-K decrease in the GFS forecast temperature in the lower troposphere results in the retrieved TPW BIAS decrease (0.26 mm at 1800 UTC) from the *GOES-13* LAP retrieval, and the 5% decrease (or 0.43 mm decrease in PW at 1800 UTC) in the GFS forecast water vapor in the lower troposphere induces the retrieved TPW BIAS decrease (0.41 mm at 1800 UTC) from the *GOES-13* LAP retrieval. From these experiments, it is clear that the background inputs affect the quality of the retrieval. And similar to the monthly variation experiments, the consistent diurnal trend of the *GOES-13* LAP TPW BIAS is still observed after the temperature/water vapor BIAS adjustment in the experiments.

The increased BIAS in the *GOES-13* LAP TPW at 1800 UTC (and possibly for July in Fig. 4 as well) may be due to the possible calibration issue in observed *GOES-13* BTs. Yu and Wu (2013) investigated the diurnal variation in the accuracy of the *GOES-13* sounder infrared channels. They compared *GOES-13* sounder BT measurements with AIRS and the Infrared Atmospheric Sounding Interferometer (IASI) hyperspectral measurements. Although their study is limited to a short period between 1 November 2011 and 31 December 2011, their results show that there are diurnal variations in the accuracy of the *GOES-13* sounder BT measurements in channels 6–8; during the daytime the mean BT difference increases until noon (around 0.4 K warmer than IASI), and during the nighttime the mean BT difference decreases until midnight (around 0.4 K colder than AIRS). These are the three channels responsible for lower-atmospheric moisture retrievals. These results indicate that the *GOES-13* LAP TPW retrieval might suffer from the radiance bias in the observation. Further investigation is needed to address this issue.

3) Comparison with the operational GOES sounder retrieval algorithms

In January 2013, the Li et al. (2008) GOES sounder retrieval algorithm replaced the method of Ma et al. (1999) in NOAA operations. Figure 8 shows the statistics (RMSE) for the comparisons of TPW from the *GOES-13* LAP, Ma et al. (1999), and Li et al. (2008) algorithms compared with the MWR TPW at the ARM CART site over 3 months between 1 June 2012 and 30 August 2012. Only these 3 months are included because the Li et al. (2008) TPWs became available starting 1 June 2012. The sample size is 715. Figure 8 clearly demonstrates the improvement in the Li et al. (2008) algorithm over Ma et al. (1999); the RMSE difference is 0.76 mm in all the 3 months. Moreover, the *GOES-13* LAP TPW shows even better results than the Li et al. (2008) algorithm; the mean RMSE difference of the 3 months between the *GOES-13* LAP and Li et al. (2008) algorithm is 0.15 mm. These results imply that the *GOES-13* ABI LAP retrieval algorithm is superior to both the current and the previous operational GOES

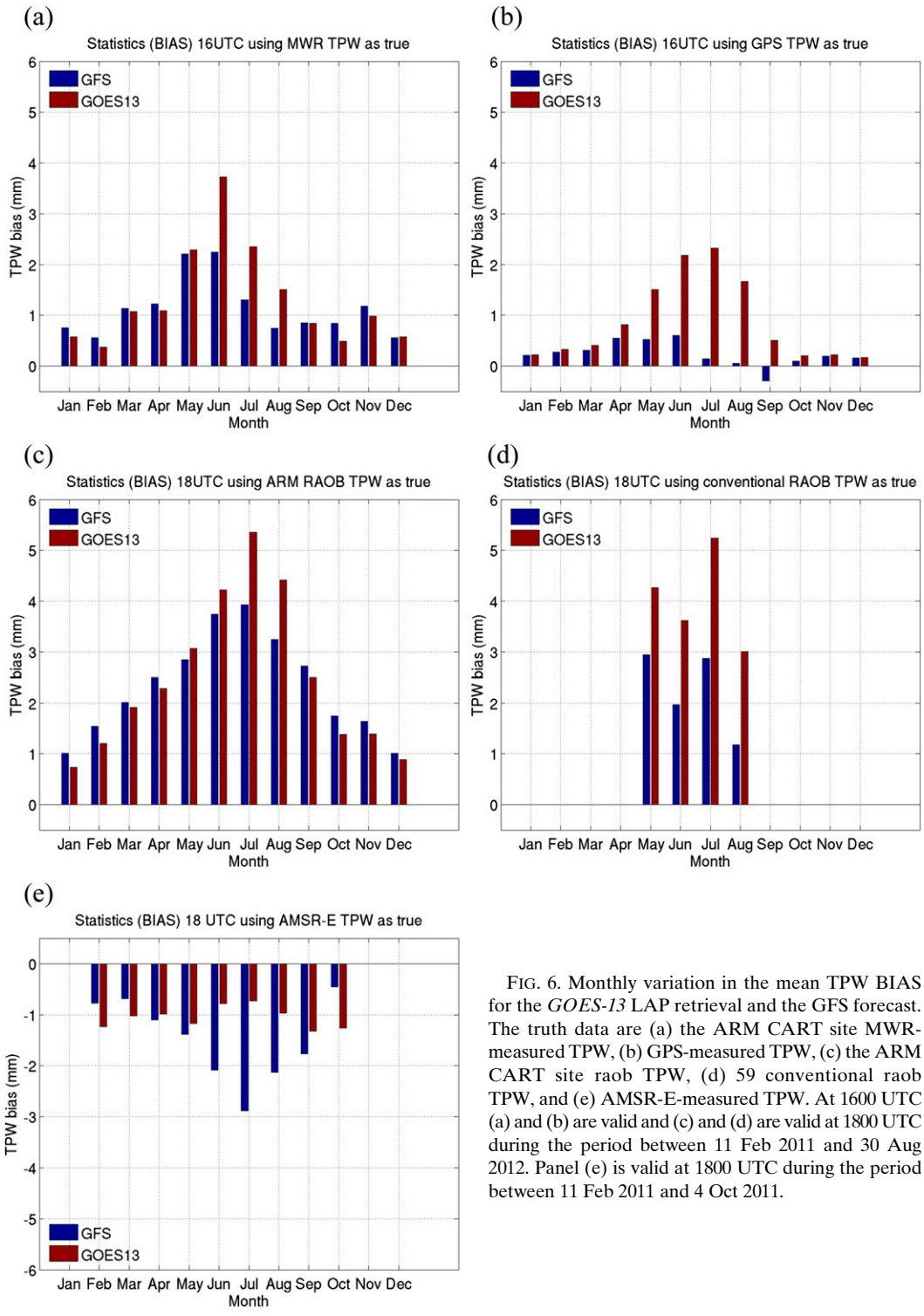

FIG. 6. Monthly variation in the mean TPW BIAS for the *GOES-13* LAP retrieval and the GFS forecast. The truth data are (a) the ARM CART site MWR-measured TPW, (b) GPS-measured TPW, (c) the ARM CART site raob TPW, (d) 59 conventional raob TPW, and (e) AMSR-E-measured TPW. At 1600 UTC (a) and (b) are valid and (c) and (d) are valid at 1800 UTC during the period between 11 Feb 2011 and 30 Aug 2012. Panel (e) is valid at 1800 UTC during the period between 11 Feb 2011 and 4 Oct 2011.

sounding algorithms for the time period in consideration. One main difference in the retrieval algorithms between this study and Li et al. (2008) is the radiative transfer model. Since the radiative transfer model plays a critical role in the cost function [Eq. (1)], some of the differences found here may be because the current LAP algorithm employs the CRTM rather than the PFAAST that was employed in Li et al. (2008). CRTM has been found to be

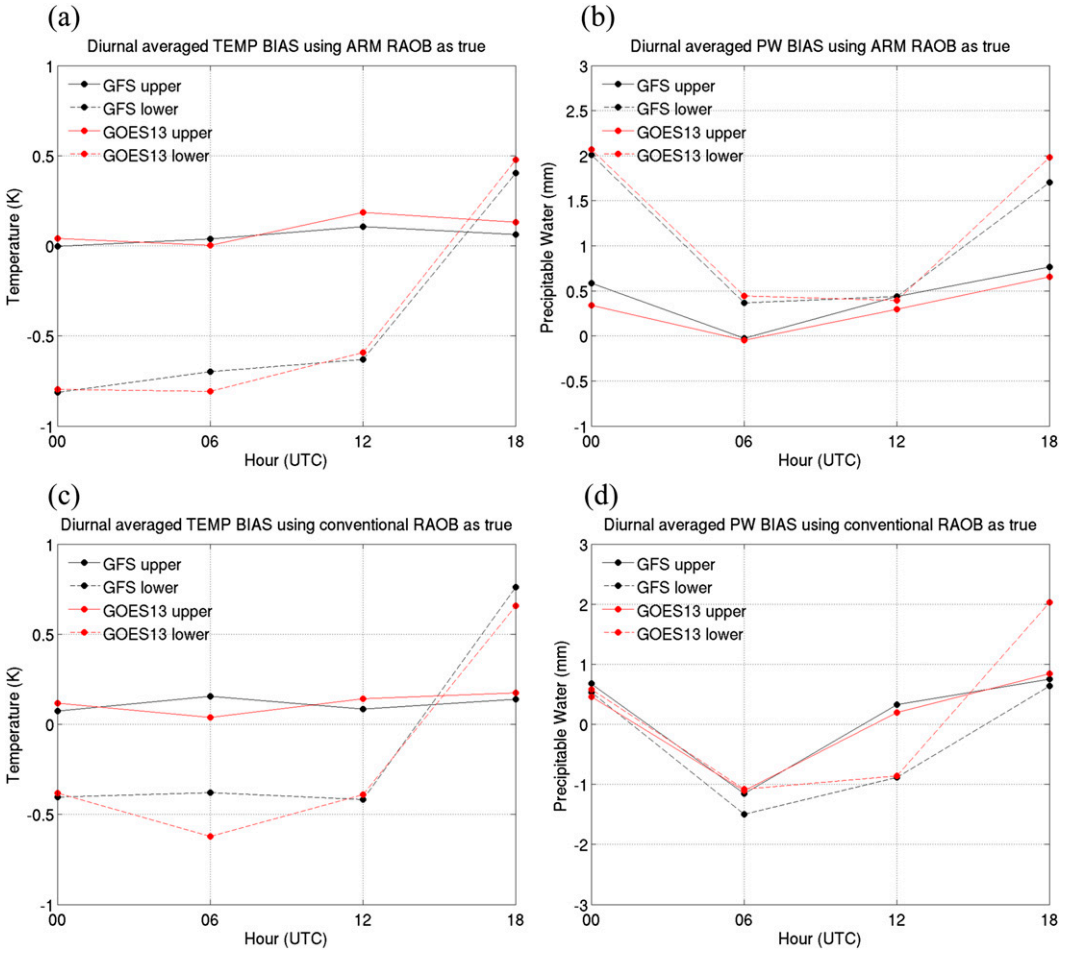

FIG. 7. As in Fig. 4, but for diurnal variation, and (a) and (b) are at the ARM CART site and (c) and (d) are at the conventional raob sites.

superior to PFAAST in brightness temperature calculation (of a moisture channel) because of the usage of the improved atmospheric transmittance model (Chen et al. 2010, 2012), which results in improved retrieval capability (Jin et al. 2011).

Since products from the GOES sounder using the *GOES-13* LAP retrieval algorithm could provide additional information not available with the current operational products, the *GOES-13* LAP algorithm will be used to develop real-time GOES sounder products at CIMSS later in 2013 and can be transferred to NOAA operations.

c. *The lifted index during the 29 June 2012 derecho*

Since the GOES sounder provides measurements with an hourly temporal resolution and a spatial resolution of 10 km, it can be very useful for short-term severe weather forecasting (Menzel et al. 1998; Li et al. 2008). The lifted index (in Celsius) calculated from the GOES sounder–retrieved atmospheric profiles can be used in severe thunderstorm forecasting to measure the atmospheric instability. Negative (positive) values of the lifted index generally represent unstable (stable) atmospheric conditions. Values between 0 and −3 indicate marginally unstable atmospheric conditions. Values between −3 and −6 indicate moderately unstable conditions. Values between −6 and −9 denote very unstable atmospheric conditions. Values less than −9 signify extreme instability.

A case study using lifted index imagery of the 29 June 2012 derecho over the Midwest and East Coast area is shown in Fig. 9. This derecho was one of the most destructive and fast-moving severe thunderstorm complexes in North American history. It resulted in 22 deaths, widespread power outages, and damage across the affected region. The storm was initiated as a small thunderstorm cell in Iowa and continued into the midwestern United States and into the mid-Atlantic states.

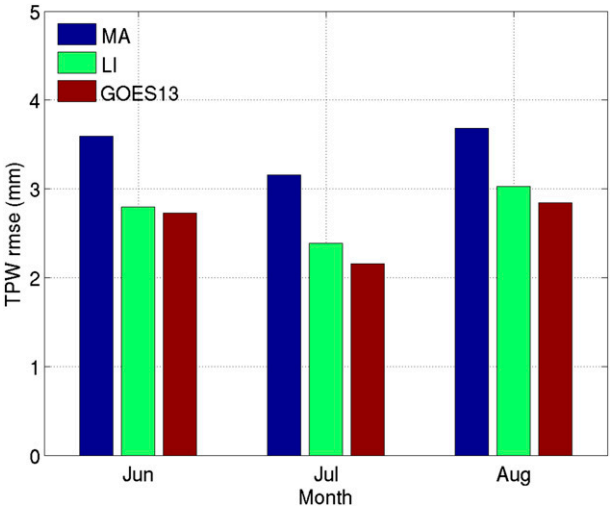

FIG. 8. Monthly variation in RMSE for TPW from the *GOES-13* LAP retrieval algorithm, Ma et al. (1999) algorithm, and Li et al. (2008) algorithm. The truth data are the MWR-measured TPW at the ARM CART site and the data are valid during the period between 1 Jun 2012 and 30 Aug 2012.

As the storm crossed into Indiana, it became a derecho and wind gusts increased substantially with a well-defined bow echo shape. Around 1900 UTC, when the storm traversed north-central Indiana, a severe thunderstorm watch with high wind probabilities was issued by the Storm Prediction Center (SPC) for large areas of Ohio and West Virginia, along with parts of Indiana and Kentucky. In addition, several tornado warnings and warnings of extreme wind threats were issued over the derecho track. The derecho crossed over the Columbus, Ohio, area at approximately 2100 UTC, with wind gusts reported as 132 km h^{-1}, which is equivalent to a category 1 hurricane. It maintained this intensity until early evening.

In Fig. 9, lifted index imagery is shown at 2100 UTC in the middle of the derecho track in order to demonstrate the application of the GOES sounding products to severe thunderstorm forecasting. Figure 9 also includes the locations of wind and hail reports by the SPC between 2130 and 2330 UTC during the derecho period while the derecho headed to the southeast. Wind and hail reports are from southeastern Ohio, northwestern West Virginia, and parts of Indiana and Kentucky. The lifted index from the *GOES-13* LAP, Li et al. (2008) and Ma et al. (1999) retrievals, and the GFS forecast at 2100 UTC are presented. The *GOES-13* LAP and Li et al. (2008) retrievals show extremely unstable areas well matched with the locations where strong winds and hail were reported, while the GFS forecast shows an unstable area over Kentucky and western West Virginia, farther south of the wind and hail report locations. The Ma et al. (1999) retrieval shows weaker instability than the *GOES-13* LAP and Li et al. (2008) retrievals over the wind and hail report locations. Note the *GOES-13* LAP provides slightly more useful information than Li et al. (2008) by revealing a more unstable environment in the storm region. With the GOES lifted index imagery, forecasters have the ability to identify regions with high instabilities with sufficient lead time prior to the outbreak of severe weather.

4. Summary

In an effort to evaluate the GOES-R ABI LAP retrieval algorithm, it is applied to the *GOES-13* sounder measurements. This study focuses on evaluating the integrated total precipitable water (TPW) as well as the temperature/water vapor profiles. The truth observations include raobs at the ARM CART site and 59 conventional raob sites, the microwave radiometer–measured TPW at the ARM CART site, the GPS-measured TPW at 251 GPS–IPW NOAA network locations over land, and the AMSR-E-measured TPW over the ocean. These truth datasets are collected over the eastern CONUS for the period between 11 February 2011 and 30 August 2012, except AMSR-E, which is collected for the period between 11 February 2011 and 4 October 2011. The GFS forecast, which is used as the background input for the physical retrieval algorithm, is included in the comparison.

The *GOES-13* LAP temperature profile shows similar statistics as the GFS forecast temperature profile, when compared with RAOBs at the ARM CART site and at the conventional raob sites. This is because 1) there are only six *GOES-13* sounder CO_2 channels sensitive to troposphere temperature used in the algorithm, and 2) the GFS forecast temperature is already good (the RMSE is less than 1 K for the troposphere between 300 and 700 hPa). However, the *GOES-13* LAP relative humidity profile RMSE is significantly improved from the GFS forecast RMSE at the vertical levels between 300 and 700 hPa with the help of three water vapor channels in the *GOES-13* sounder measurements. These results confirm that the LAP algorithm meets the GOES-R program requirements.

Monthly TPW comparison with five truth datasets shows that the *GOES-13* LAP TPW consistently reduces RMSE from the GFS forecast TPW with only a few exceptions (July with the raob TPW at the ARM CART site and February and October with the AMSR-E TPW). Experiments verified that the algorithm is sensitive to the quality of the background (GFS forecast fields in this study).

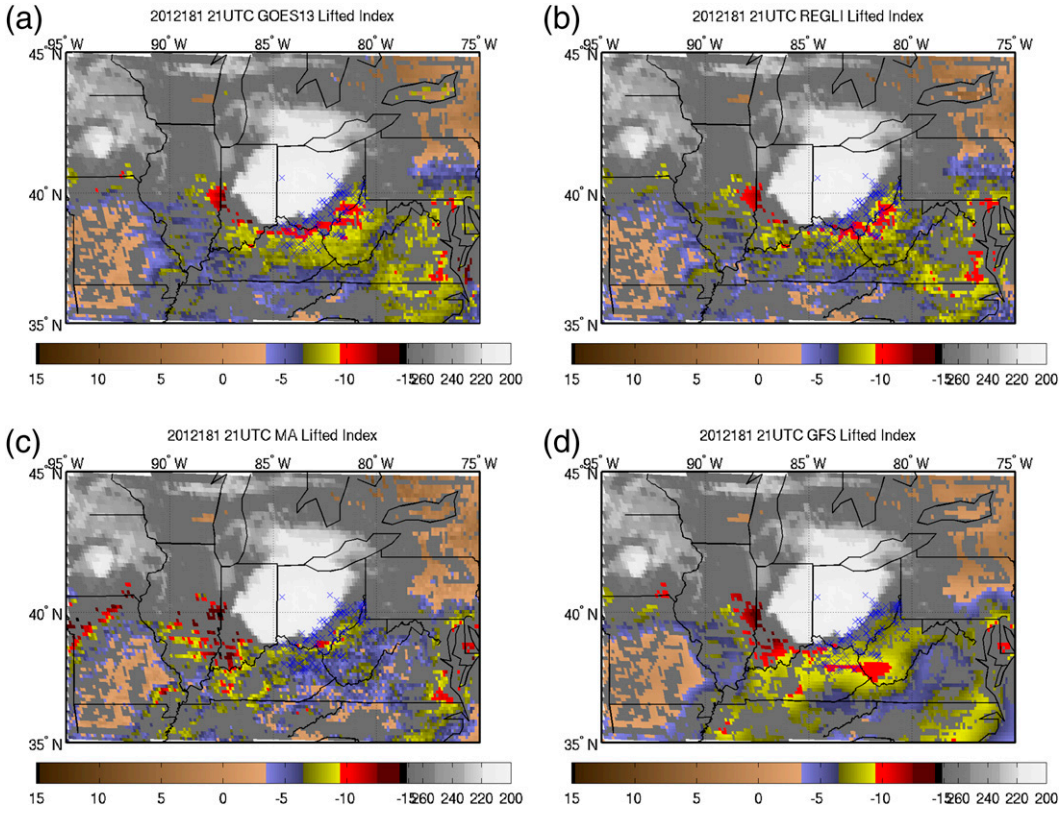

FIG. 9. Wind and hail reports (blue cross) between 2130 and 2330 UTC on 29 Jun 2012 and lifted index for clear skies with brightness temperature for cloudy skies (*GOES-13* sounder channel 8, gray color bar) at 2100 UTC on 29 Jun 2012 during a derecho. (a) *GOES-13* LAP retrieval, (b) Li et al. (2008) retrieval, (c) Ma et al. (1999) retrieval, and (d) NCEP GFS forecast.

Diurnal TPW comparisons show that most RMSE and all STD values are reduced in the *GOES-13* LAP TPW from the GFS forecast TPW. However, during the daytime (especially near 1800 UTC), the RMSE differences between the LAP TPW retrievals over land and those from the GFS were found to be insignificant relative to the truth data. This is likely due to the corresponding increase in the LAP TPW BIAS relative to the GFS owing to issues with the *GOES-13* radiance calibration.

Since the GOES satellites observe North America, the GOES-R ABI LAP algorithm should be validated over North America. Note that the GOES sounder is the only real proxy data for the validation over this region that SEVIRI does not cover. This study is the first try with the GOES-R ABI LAP algorithm applied to the current GOES sounder over CONUS.

Jin et al. (2008) and Xie et al. (2013) showed that statistical plots of the temperature difference between NCEP GFS (or ECMWF) and the retrieval have similar patterns given that the retrieval depends on the first guess derived through a regression based on NCEP GFS (or ECMWF) forecast data and also showed that the retrievals generally improve the moisture profiles compared to the background (NCEP GFS or ECMWF forecast), which are clearly demonstrated in this study. As Schmit et al. (2008) revealed that both the current GOES sounder and ABI-like retrievals can provide additional moisture information, Jin et al. (2008), Xie et al. (2013), and this study all show that the retrievals, using all the channels of the current GOES sounder or ABI-like channels, work more effectively on moisture rather than on temperature.

From this study, the quality of the *GOES-13* LAP products (temperature/water vapor profiles and TPW) is reasonable and stable. The capability of the GOES-R ABI LAP retrieval algorithm revealed in this study and a previous study (Jin et al. 2008) indicates that the GOES-R ABI LAP retrieval algorithm using the GOES-R ABI instrument is well prepared to provide the continuity of the current GOES sounder measurements to make up the gap until any new geostationary advanced infrared sounder is launched.

The GOES-R ABI LAP retrieval algorithm has been applied to MODIS measurements and planned to be

launched on the International MODIS/AIRS Processing Package (IMAPP), which is publicly available and accessed from more than 60 countries. The GOES-R ABI LAP retrieval algorithm is also planned to be implemented in the Geostationary Cloud Algorithm Testbed (GEOCAT) for real-time GOES sounder processing.

Acknowledgments. This work was funded under the National Oceanic and Atmospheric Administration Cooperative Agreement NA10NES4400013. The authors thank J. Nelson for the help to prepare *GOES-13* sounder and related truth data. The views, opinions, and findings contained in this report are those of the author(s) and should not be construed as an official National Oceanic and Atmospheric Administration or U.S. government position, policy, or decision.

REFERENCES

Birkenheuer, D. L., and S. I. Gutman, 2005: A comparison of GOES moisture-derived product and GPS-IPW data during IHOP-2002. *J. Atmos. Oceanic Technol.,* **22,** 1838–1845.

Chen, S. H., Z. Zhao, J. S. Haase, A. Chen, and F. Vandenberghe, 2008: A study of the characteristics and assimilation of retrieved MODIS total precipitable water data in severe weather simulations. *Mon. Wea. Rev.,* **136,** 3608–3628.

Chen, Y., Y. Han, P. Van Delst, and F. Weng, 2010: On water vapor Jacobian in fast radiative transfer model. *J. Geophys. Res.,* **115,** D12303, doi:10.1029/2009JD013379.

——, ——, and F. Weng, 2012: Comparison of two transmittance algorithms in the Community Radiative Transfer Model: Application to AVHRR. *J. Geophys. Res.,* **117,** D06206, doi:10.1029/2011JD016656.

Collard, A., and Coauthors, 2010: An overview of the assimilation of AIRS and IASI radiances at operational NWP centres. *Proc. 17th Int. TOVS Study Conf.,* Monterey, CA, TOVS Working Group, 7.9. [Available online at http://cimss.ssec.wisc.edu/itwg/itsc/itsc17/session7/7.9_collard.pdf.]

Dai, A., F. Giorgi, and K. E. Trenberth, 1999: Observed and model-simulated precipitation diurnal cycle over the contiguous United States. *J. Geophys. Res.,* **104** (D6), 6377–6402.

——, J. Wang, R. H. Ware, and T. Van Hove, 2002: Diurnal variation in water vapor over North America and its implications for sampling errors in radiosonde humidity. *J. Geophys. Res.,* **107,** 4090, doi:10.1029/2001JD000642.

Daniels, J. M., T. J. Schmit, and D. W. Hiller, 2001: GOES-11 science test: GOES-11 imager and sounder radiance and product validations. NOAA Tech. Rep. NESDIS 103, 49 pp.

Fetzer, E. J., B. H. Lambrigtsen, A. Eldering, H. H. Aumann, and M. T. Chahine, 2006: Biases in total precipitable water vapor climatologies from Atmospheric Infrared Sounder and Advanced Microwave Scanning Radiometer. *J. Geophys. Res.,* **111,** D09S16, doi:10.1029/2005JD006598.

Fuelberg, H. E., and S. R. Olson, 1991: An assessment of VAS derived retrievals and parameters used in thunderstorm forecasting. *Mon. Wea. Rev.,* **119,** 795–814.

Hanesiak, J., M. Melsness, and R. Raddatz, 2010: Observed and modeled growing-season diurnal precipitable water vapor in south-central Canada. *J. Appl. Meteor. Climatol.,* **49,** 2301–2314.

Hillger, D. W., and T. J. Schmit, 2010: The GOES-14 science test: Imager and sounder radiance and product validations. NOAA Tech. Rep. NESDIS 131, 120 pp.

——, ——, and J. M. Daniels, 2003: Imager and sounder radiance and product validations for the GOES-12 science test. NOAA Tech. Rep. NESDIS 115, 66 pp.

Immler, F. J., J. Dykema, T. Gardiner, D. N. Whiteman, P. W. Thorne, and H. Vomel, 2010: Reference quality upper-air measurements: Guidance for developing GRUAN data products. *Atmos. Meas. Tech.,* **3,** 1217–1231.

Jin, X., J. Li, T. J. Schmit, J. Li, M. D. Goldberg, and J. J. Gurka, 2008: Retrieving clear-sky atmospheric parameters from SEVIRI and ABI infrared radiances. *J. Geophys. Res.,* **113,** D15310, doi:10.1029/2008JD010040.

——, ——, ——, and M. D. Goldberg, 2011: Evaluation of radiative transfer models in atmospheric profiling with broadband infrared radiance measurements. *Int. J. Remote Sens.,* **32,** 863–874.

Kazumori, M., T. Egawa, and K. Yoshimoto, 2012: A retrieval algorithm of atmospheric water vapor and cloud liquid water for AMSR-E. *Eur. J. Remote Sens.,* **45,** 63–74.

Li, J., W. Wolf, W. P. Menzel, W. Zhang, H.-L. Huang, and T. H. Achtor, 2000: Global soundings of the atmosphere from ATOVS measurements: The algorithm and validation. *J. Appl. Meteor.,* **39,** 1248–1268.

——, T. J. Schmit, X. Jin, and G. Martin, 2010: GOES-R Advanced Baseline Imager (ABI) algorithm theoretical basis document for legacy atmospheric moisture profile, legacy atmospheric temperature profile, total precipitable water, and derived atmospheric stability indices. NOAA NESDIS Center for Satellite Applications and Research Rep., 106 pp. [Available online at http://www.goes-r.gov/products/ATBDs/baseline/Sounding_LAP_v2.0_no_color.pdf.]

Li, Z., J. Li, W. P. Menzel, T. J. Schmit, J. P. Nelson III, J. Daniels, and S. A. Ackerman, 2008: GOES sounding improvement and applications to severe storm nowcasting. *Geophys. Res. Lett.,* **35,** L03806, doi:10.1029/2007GL032797.

——, ——, ——, J. P. Nelson III, T. J. Schmit, E. Weisz, and S. A. Ackerman, 2009: Forecasting and nowcasting improvement in cloudy regions with high temporal GOES sounder infrared radiance measurements. *J. Geophys. Res.,* **114,** D09216, doi:10.1029/2008JD010596.

Liljegren, J. C., 1995: Observations of total column precipitable water vapor and cloud liquid water using a dual-frequency microwave radiometer. *Microwave Radiometry and Remote Sensing of the Environment,* D. Solimini, Ed., Vista Science Press, 107–118.

Liu, Y.-C., S.-H. Chen, and F.-C. Chien, 2011: Impact of MODIS and AIRS total precipitable water on modifying the vertical shear and Hurricane Emily simulations. *J. Geophys. Res.,* **116,** D02126, doi:10.1029/2010JD014528.

Ma, X. L., T. Schmit, and W. L. Smith, 1999: A nonlinear physical retrieval algorithm—Its application to the *GOES-8/9* sounder. *J. Appl. Meteor.,* **38,** 501–513.

Mattioli, V., R. Westwater, S. I. Gutman, and V. R. Morris, 2005: Forward model studies of water vapor using scanning microwave radiometers, global positioning system, and radiosondes during the cloudiness intercomparison experiment. *IEEE Trans. Geosci. Remote Sens.,* **43,** 1012–1021.

Menzel, W. P., and J. F. W. Purdom, 1994: Introducing GOES-I: The first of a new generation of Geostationary Operational Environmental Satellites. *Bull. Amer. Meteor. Soc.,* **75,** 757–781.

——, F. C. Holt, T. J. Schmit, R. M. Aune, T. J. Schreiner, G. S. Wade, and D. Gray, 1998: Application of *GOES-8/9* soundings to weather forecasting and nowcasting. *Bull. Amer. Meteor. Soc.,* **79,** 2059–2077.

Pacione, R., E. Fionda, R. Ferrara, R. Lanotte, C. Sciarretta, and F. Vespe, 2002: Comparison of atmospheric parameters derived from GPS, VLBI and a ground-based microwave radiometer in Italy. *Phys. Chem. Earth,* **27,** 309–316.

Rao, P. A., and H. E. Fuelberg, 1998: An evaluation of *GOES-8* retrievals. *J. Appl. Meteor.,* **37,** 1577–1587.

Reale, T., B. Sun, F. H. Tilley, and M. Pettey, 2012: The NOAA Products Validation System (NPROVS). *J. Atmos. Oceanic Technol.,* **29,** 629–645.

Rodgers, C. D., 1976: Retrieval of atmospheric temperature and composition from remote measurements of thermal radiation. *Rev. Geophys. Space Phys.,* **14,** 609–624.

Schmit, T. J., W. F. Feltz, W. P. Menzel, J. Jung, A. P. Noel, J. N. Heil, J. P. Nelson III, and G. S. Wade, 2002: Validation and use of GOES sounder moisture information. *Wea. Forecasting,* **17,** 139–154.

——, M. M. Gunshor, W. P. Menzel, J. J. Gurka, J. Li, and S. Bachmeier, 2005: Introducing the next-generation Advanced Baseline Imager (ABI) on GOES-R. *Bull. Amer. Meteor. Soc.,* **86,** 1079–1096.

——, J. Li, J. J. Gurka, M. D. Goldberg, K. J. Schrab, J. Li, and W. F. Feltz, 2008: The GOES-R Advanced Baseline Imager and the continuation of current sounder products. *J. Appl. Meteor. Climatol.,* **47,** 2696–2711.

——, ——, S. A. Ackerman, and J. J. Gurka, 2009: High-spectral- and high-temporal-resolution infrared measurements from geostationary orbit. *J. Atmos. Oceanic Technol.,* **26,** 2273–2292.

Schrab, K. J., 1998: Monitoring the southwest U. S. summer monsoon using GOES-9 data. Preprints, *16th Conf. on Weather Analysis and Forecasting,* Phoenix, AZ, Amer. Meteor. Soc., 368–369.

Schreiner, A. J., T. J. Schmit, and W. P. Menzel, 2001: Observations and trends of clouds based on GOES sounder data. *J. Geophys. Res.,* **106** (D17), 20 349–20 363.

Seemann, S. W., J. Li, W. P. Menzel, and L. E. Gumley, 2003: Operational retrieval of atmospheric temperature, moisture, and ozone from MODIS infrared radiances. *J. Appl. Meteor.,* **42,** 1072–1091.

——, E. E. Borbas, R. O. Knuteson, G. R. Stephenson, and H.-L. Huang, 2008: Development of a global infrared land surface emissivity database for application to clear sky sounding retrievals from multispectral satellite radiance measurements. *J. Appl. Meteor. Climatol.,* **47,** 108–203.

Sieglaff, J. M., T. J. Schmit, W. P. Menzel, and S. A. Ackerman, 2009: Inferring convective weather characteristics with geostationary high spectral resolution IR window measurements: A look into the future. *J. Atmos. Oceanic Technol.,* **26,** 1527–1541.

Stokes, G. M., and S. E. Schwartz, 1994: The Atmospheric Radiation Measurement (ARM) program: Programmatic background and design of the Cloud and Radiation Testbed. *Bull. Amer. Meteor. Soc.,* **75,** 1201–1221.

Turner, D. D., B. M. Lesht, S. A. Clough, J. C. Liljegren, H. E. Revercomb, and D. C. Tobin, 2003: Dry bias and variability in Vaisala RS80-H radiosondes: The ARM experience. *J. Atmos. Oceanic Technol.,* **20,** 117–132.

Velden, C. S., C. M. Hayden, S. J. Nieman, W. P. Menzel, S. Wanzong, and J. S. Goerss, 1997: Upper-tropospheric winds derived from geostationary satellite water vapor observations. *Bull. Amer. Meteor. Soc.,* **78,** 173–195.

Wang, J., A. Dai, D. J. Carlson, R. H. Ware, and J. C. Liljegren, 2002: Diurnal variation in water vapor and liquid water profiles from a new microwave radiometer profiler. Preprints, *Sixth Symp. on Integrated Observing Systems,* Orlando, FL, Amer. Meteor. Soc., 5.5. [Available online at http://ams.confex.com/ams/pdfpapers/27917.pdf.]

Weng, F., Y. Han, P. van Delst, Q. Liu, and B. Yan, 2005: JCSDA Community Radiative Transfer Model (CRTM). *Proc. 14th Int. TOVS Study Conf.,* Beijing, China, TOVS Working Group, 217–222. [Available online at http://library.ssec.wisc.edu/research_Resources/publications/pdfs/ITSC14/weng02_ITSC14_2005.pdf.]

Xie, H. N. R., and Coauthors, 2013: Integration and ocean-based prelaunch validation of GOES-R Advanced Baseline Imager legacy atmospheric products. *J. Atmos. Oceanic Technol.,* **30,** 1743–1756.

Yu, F., and X. Wu, 2013: Radiometric calibration accuracy of GOES sounder infrared channels. *IEEE Trans. Geosci. Remote Sens.,* **51,** 1187–1199.